CORA Cork Open Research Archive
Cartlann Taighde Oscailte Chorcaí

Title	Improvement in biohydrogen and volatile fatty acid production from seaweed through addition of conductive carbon materials depends on the properties of the conductive materials
Authors	Deng, Chen;Lin, Richen;Kang, Xihui;Wu, Benteng;Wall, David M.;Murphy, Jerry D.
Publication date	2022
Original Citation	Deng, C., Lin, R., Kang, X., Wu, B., Wall, D. M. and Murphy, J. D. (2022) 'Improvement in biohydrogen and volatile fatty acid production from seaweed through addition of conductive carbon materials depends on the properties of the conductive materials', Energy, 239, 122188 (16pp). doi: 10.1016/j.energy.2021.122188
Type of publication	Article (peer-reviewed)
Link to publisher's version	10.1016/j.energy.2021.122188
Rights	© 2021 The Author(s). Published by Elsevier Ltd. This is an open access article under the CC BY license (http://creativecommons.org/licenses/by/4.0/). - https://creativecommons.org/licenses/by/4.0/
Download date	2026-11-17 12:31:44
Item downloaded from	https://hdl.handle.net/10468/13401

UCC
University College Cork, Ireland
Coláiste na hOllscoile Corcaigh

Energy 239 (2022) 122188

Contents lists available at ScienceDirect

Energy

journal homepage: www.elsevier.com/locate/energy

Improvement in biohydrogen and volatile fatty acid production from seaweed through addition of conductive carbon materials depends on the properties of the conductive materials

Chen Deng [a, b], Richen Lin [a, b, *], Xihui Kang [a, b], Benteng Wu [a, b], David Wall [a, b], Jerry D. Murphy [a, b]

[a] MaREI Centre, Environmental Research Institute, University College Cork, Cork, Ireland
[b] Civil, Structural and Environmental Engineering, School of Engineering and Architecture, University College Cork, Cork, Ireland

ARTICLE INFO

Article history:
Received 12 July 2021
Received in revised form
7 September 2021
Accepted 25 September 2021
Available online 28 September 2021

Keywords:
Biohydrogen
Carbonaceous materials
Biochar
Graphene
Electron transfer

ABSTRACT

Fermentative production of biohydrogen and volatile fatty acids (VFAs) from advanced feedstocks such as seaweed provides opportunities in the carbon-neutral bioeconomy. The gap in the state of the art exists in overcoming both the low fermentation efficiency associated with the rigid structure of seaweed and the inefficient metabolic electron transfer within the microbial communities. This study evaluated the effects of carbonaceous additives (such as graphene and various biochars) on biohydrogen fermentation of glucose, cellulose, and the brown seaweed *Laminaria digitata*. The impacts of carbonaceous additives varied significantly in terms of hydrogen production, VFA profiles, and microbial communities. Graphene and wood-derived biochar (Wood_Biochar) were shown to be superior to draff-derived biochars. In the fermentation of *L. digitata*, graphene and Wood_Biochar significantly reduced the lag-phase time by 47% and 49%, respectively. Microbial analysis revealed that the enhanced fermentation was ascribed to the enrichment of *Thermoanaerobacterium* genus in response to carbonaceous additives. Kinetic correlations between the fermentation parameters and the properties of the additives suggested that the graphitic structure and electrical conductivity might play a crucial role in facilitating the fermentation. The mechanisms might be ascribed to (1) the supported biofilm growth and (2) enhancement in microbial electron transfer induced by the additives.
© 2021 The Author(s). Published by Elsevier Ltd. This is an open access article under the CC BY license (http://creativecommons.org/licenses/by/4.0/).

1. Introduction

Hydrogen is enjoying rapidly growing attention globally as an energy vector that can help achieve carbon neutrality. It offers solutions to decarbonise hard-to-decarbonise sectors such as heavy transport and the steel industry. In strategies to reach carbon neutrality by 2050, the European Union projected the share of hydrogen in its energy mix to grow from less than 2% in 2019 to 13–14% by 2050 [1]. Hydrogen can not only be used as a compressed gaseous fuel in engines or fuel cells but also as a feedstock for the production of synthetic fuels (such as multi-carbon alkanes/alkenes) for application in heavy-duty vehicles, aviation and shipping where other alternatives (such as electricity) are not amenable. For example, hydrogen can react with CO_2 in biogas via methanation to create carbon-neutral methane if the hydrogen used is renewable [2].

However, the emissions associated with hydrogen or hydrogen-derived synthetic fuels depend on the production technologies. Currently, hydrogen is still largely produced from fossil fuels, primarily natural gas or coal, and is responsible for the release of 70–100 million tonnes of CO_2 per year (corresponding to an annual consumption of 9.7 million tonnes of hydrogen) in Europe [1,3]. For hydrogen to contribute to climate neutrality, its production must be carbon neutral or significantly decarbonised. Three approaches to renewable hydrogen production are currently suggested in the literature: electrolysis of water using renewable electricity; biogas reforming; and biochemical conversion of biomass. Among the biochemical conversion technologies, one predominant option is dark hydrogen fermentation. Through microbial metabolism, a wide range of biomass can be fermented to hydrogen, carbon dioxide and volatile fatty acids (VFAs). The VFAs are valuable platform

* Corresponding author. MaREI Centre, Environmental Research Institute, University College Cork, Ireland.
E-mail address: richen.lin@ucc.ie (R. Lin).

https://doi.org/10.1016/j.energy.2021.122188
0360-5442/© 2021 The Author(s). Published by Elsevier Ltd. This is an open access article under the CC BY license (http://creativecommons.org/licenses/by/4.0/).

chemicals that can be converted to medium-chain carboxylic acids and further valorised to lightweight bio-alkanes through different bio-based technologies [4]. Besides standing alone as a hydrogen production process, hydrogen fermentation also has a strong potential to integrate with different biochemical processes (such as microbial CO_2 electrosynthesis) in a modern carbon-neutral circular bioeconomy [5–7].

The search for feasible substrates for fermentative hydrogen production has been extensively investigated, including for energy crops, grass, food waste, and seaweed [14,15]. Not all biomass resources are considered sustainable when the carbon footprint associated with the cultivation, harvesting, processing, and transportation are taken into account. Compared to terrestrial biomass, seaweed offers some advantages including fast and efficient photosynthetic growth, lack of competition with food crops for arable land and freshwater, high carbohydrate content, and low lignin content. Brown seaweed species (common kelp) such as *Laminaria japonica* (*L. japonica*) and *Laminaria digitata* (*L. digitata*) are promising fermentable substrates due to the presence of readily fermentable sugars and the large potential for seaweed yield [16]. The EU hydrogen strategy highlights the low technology readiness level of hydrogen production from seaweed [1]. Table 1 summarises the reported studies of fermentative biohydrogen production from *Laminaria* species. The literature would suggest that hydrogen yields obtained from *L. japonica* and *L. digitata* (Table 1) are in the range of 6–80 ml/g based on volatile solids (VS) or total solids (TS). However, based on the organic components of *Laminaria* species, the theoretical hydrogen yield was estimated to be in the range of 407.0–477.9 mL H_2/g VS [17]. As such the conversion efficiency of brown seaweed is low at the current technology level. This may be attributed to the rigid cell wall of seaweed which makes the intracellular components difficult to be accessed by the hydrogen-producing bacteria [18]. Previous studies primarily focused on mesophilic (25–40 °C) fermentation of seaweed for biohydrogen production. Nevertheless, higher biohydrogen yield may be achieved under thermophilic conditions (40–65 °C) as thermophilic hydrogen-producing bacteria exhibit higher inhibitor tolerance and faster metabolic activities [17,19]. To date, the authors could not find any study in the literature that has reported fermentative biohydrogen production from seaweed under thermophilic conditions.

Fermentative biohydrogen production from seaweed must be improved in a cost-efficient way to achieve economic and environmental sustainability. Pre-treatment of the substrate is widely investigated to improve biohydrogen yield, however, it requires an additional input of energy and chemicals [20]. Supplementation of additives to enhance anaerobic fermentation has attracted increasing attention due to ease of operation and low energy consumption [21,22]. The most investigated additives include metal monomers, metal oxides, and carbon materials such as activated carbon and biochar [23–25]. Carbon materials have been applied to enhance the fermentation of glucose, sewage sludge, and food waste, and have led to encouraging enhancement in biohydrogen production [26,27]. As reviewed in Table 10 (in section 3.6), carbon cloth, activated carbon, and various biochars increased the biohydrogen yield from glucose by 26.6–49%, increased the acetate yield by up to100%, and simultaneously reduced the lag-phase time [28–31]. The enhancing effects of these carbon materials were attributed to the promotion of biofilm growth, the facilitation of syntrophic growth of fermentative bacteria and homoacetogens, and the maintenance of pH [26]. The large-molecular-weight carbohydrate polymers such as alginate, fucoidan, laminarin, and agar in seaweed cannot be readily degraded into easily fermentable monomers such as glucose, galactose, and mannose, leading to the relatively low biodegradability. The effects of conductive carbon materials on the fermentation performance of seaweed may be distinct from the fermentation of other feedstocks due to the recalcitrance of the seaweed structure. To the best of the authors' knowledge, studies on enhancing biohydrogen fermentation of seaweed with carbon materials have not been reported in previous literature.

The innovation in this study is that it is the first to assess the potential enhancing effects of carbon additives on fermentative biohydrogen and VFAs co-production from seaweed under thermophilic conditions. To better understand how the carbon additives affect the degradation of different components in seaweed, a readily degradable monosaccharide glucose and a typical hard-to-ferment polysaccharide cellulose were also utilised as the model substrates for hydrogen fermentation. The specific objectives of this study are to (1) comparatively investigate the physicochemical properties of different carbon materials including expensive graphene and low-cost biochars; (2) evaluate the feasibility of enhancing fermentative biohydrogen and VFA production from monosaccharide (glucose), polysaccharide (cellulose), and seaweed with different carbon materials; (3) identify the key properties of carbon materials contributing to the enhancing effects. The results of this study may technically contribute to the development of green hydrogen production via biochemical conversions.

2. Materials and methods

2.1. Materials

2.1.1. Fermentation inoculum

The seed inoculum for the cultivation of hydrogen-producing bacteria was from an anaerobic digester in the lab treating cattle manure and cellulose. Firstly, the seed inoculum was heated at 100 °C in an autoclave for 30 min to inactivate methanogens. Subsequently, the treated inoculum was acclimated three times at 55 °C to enrich the thermophilic spore-forming hydrogenogens using a modified culture medium [32]. Finally, the fermentation inoculum was degassed for 3 days before the biohydrogen potential assays.

2.1.2. Feedstock

Glucose and cellulose used for biohydrogen and VFAs

Table 1
A review of studies focusing on fermentative biohydrogen production from brown seaweed without pre-treatment.

Seaweed species	Batch/ Continuous	Feedstock loading	Fermentation temperature (°C)	Inoculum	H_2 yield	VFA yield	Reference
L. japonica	Batch	10 g TS/L	35	Sewage sludge (65 °C heated)	44 ml/g TS	\	[8]
L. digitata	Continuous	12 g VS/L/d	37	Mixed fermentation bacteria (100 °C heated)	26 ml/g VS	6511.7 mg/L	[9]
Dried *L. japonica*	Batch	21 g TS/L	35	Mixed fermentation bacteria (90 °C heated)	5.7 ml/g TS	\	[10]
Dried *L. japonica*	Batch	10 g TS/L	35	Mixed fermentation bacteria (80 °C heated)	10 ml/g TS	\	[11]
Dried *L. digitata*	Batch	10 g VS/L	35	Sludge from swine slurry (100 °C heated)	35.7 ml/g VS	2550 mg/L	[12]
Dried *L. digitata*	Batch	\	37	Mixed fermentation bacteria (100 °C heated)	79.6 ml/g VS	\	[13]

production were purchased from Sigma Aldrich. The seaweed feedstock *L. digitata* was naturally harvested in May from a beach in West Cork, Ireland. The seaweed was minced into pieces of less than 4 mm in size and frozen before use [5].

2.1.3. Carbonaceous materials

Four carbon materials were assessed as additives to enhance fermentative biohydrogen production. The graphene powder was purchased from Sigma Aldrich and its particle size was 2 μm. Draff_N_2_Biochar and Draff_CO_2_Biochar were produced in a compact tube furnace (R50/250/12, Nabertherm, Germany) in the lab through pyrolysis of draff (a solid by-product from whiskey production) at 700 °C. Draff_N_2_Biochar was produced in a N_2 atmosphere and Draff_CO_2_Biochar was produced in a CO_2 atmosphere. Wood_Biochar was provided by a local plant pyrolyzing wood waste at 700 °C in a rotary kiln system [5]. The three types of biochar samples were ground into powders with a particle size smaller than 150 μm. All the carbon materials were oven-dried overnight at 105 °C before application.

2.2. Methods

2.2.1. Biohydrogen potential assays

The biohydrogen potential assays were conducted in the Bioprocess Automatic Methane Potential Test System (APMTS II, Bioprocess Control, Sweden) [5]. To evaluate the effects of different carbon additives on biohydrogen production from glucose, cellulose, and *L. digitata*, sixteen groups of fermentation experiments were conducted (Table 2). Each experimental group was tested in triplicate. Group 0 was a blank group containing only the inoculum to evaluate the gas and VFA production from the inoculum. The production of biohydrogen and VFAs in other experimental groups were all standardised by subtracting the data from Group 0. Group 1 to Group 5 were set up for the biohydrogen potential assay of glucose with/without the addition of carbon materials. Group 6 to Group 10 were set up for the biohydrogen potential assay of cellulose with/without the addition of carbon materials. Group 11 to Group 15 were set up for the biohydrogen potential assay of *L. digitata* with/without the addition of different carbon materials.

To set up the experimental process firstly, the feedstock containing 2 g VS was added into each reactor except the reactors in Group 0, and subsequently the carbon additives were added. After the addition of additives, 20 ml of fermentation inoculum were added into each reactor. Distilled water was used to adjust the total working volume in each reactor to 200 ml (resulting in a headspace of 450 ml). The initial pH in each reactor was adjusted to 7.0 ± 0.05 with 1 M NaOH and 1 M HCl solutions. All reactors were completely purged with N_2 and then sealed to make an anaerobic environment. The temperature of the reactors was maintained at 55 °C using a water bath. The fermentation liquid in each reactor was sampled every day to allow the analysis of the VFAs. The VFAs in the effluents were quantified using a gas chromatography system (Agilent 7890 B, USA) with configurations detailed previously [33].

The statistical analysis of differences between experimental data from all groups was conducted according to the one-way ANOVA method using the IBM SPSS Statistics V26 software. The difference was considered significant when $p < 0.05$.

2.2.2. Characterisation of materials

The proximate analysis of the feedstock and fermentation inoculum were conducted according to the 2540G methods [34]. The weight percentages of each element were measured using an elemental analyser (Elemantar Vario EL cube). The pH value of the carbon materials was measured in the suspension using a pH meter (Mettler Toledo FiveEasy F20). The suspension was made by dispersing 1.0 g of the powder into 10.0 ml of distilled water.

The electrical conductivity (EC) of solid carbon materials was measured using a bespoke conductivity meter following the method described in Ref. [35]. Briefly, the powder of each carbon material (1 g) was firstly washed three times with 1 M NaCl (5 ml) solution and centrifuged at 8000 rpm for 5 min. The supernatant was then disposed of, and the sediment pellet was collected to fill the non-conductive gap (25 mm × 0.5 mm × 0.1 mm) between two gold electrodes. A voltage ramp from −0.3 V to 0.3 V with a ramp rate of 25 mV/s was applied to the two gold electrodes using an electrochemical workstation (Biologic VSP, France) with three probes. The current-voltage curve was established according to the recorded time average current of the applied voltage. The slope of the current-voltage curve was used to calculate the EC as per the following formula (Eq. (1)):

$$\sigma = L/RS \quad \text{(Eq. 1)}$$

in which σ is the conductivity (S/m), L is the width of the non-conductive gap (0.5×10^{-3} m), S is the cross-sectional area of the gap (2.5×10^{-6} m^2), and R is the reciprocal of the slope of the current-voltage curve.

N_2 adsorption-desorption isotherms were recorded on a Micrometrics ASAP 2460 analyser. The specific surface area and

Table 2
Experimental set-up of biohydrogen potential assays.

Group No.	Feedstock		Inoculum	Carbon additive		Total working volume
	Type	Amount (g VS)	Amount (ml)	Type	Dosage (g)	Volume (ml)
Group 0	\	\	20	\	\	200
Group 1	Glucose	2	20	Graphene	0.2	200
Group 2	Glucose	2	20	Draff_N_2_Biochar	0.2	200
Group 3	Glucose	2	20	Draff_CO_2_Biochar	0.2	200
Group 4	Glucose	2	20	Wood_Biochar	0.2	200
Group 5	Glucose	2	20	\	\	200
Group 6	Cellulose	2	20	Graphene	0.2	200
Group 7	Cellulose	2	20	Draff_N_2_Biochar	0.2	200
Group 8	Cellulose	2	20	Draff_CO_2_Biochar	0.2	200
Group 9	Cellulose	2	20	Wood_Biochar	0.2	200
Group 10	Cellulose	2	20	\	\	200
Group 11	*L. digitata*	2	20	Graphene	0.2	200
Group 12	*L. digitata*	2	20	Draff_N_2_Biochar	0.2	200
Group 13	*L. digitata*	2	20	Draff_CO_2_Biochar	0.2	200
Group 14	*L. digitata*	2	20	Wood_Biochar	0.2	200
Group 15	*L. digitata*	2	20	\	\	200

porosity were obtained via the Brunauer Emmett-Teller (BET) and t-plot methods. The surface functional groups on the carbon materials were qualitatively identified on a Fourier transform infrared spectrometer (FTIR, Thermo Scientific Nicolet 10). To semi-quantitatively analyse the surface functional groups, the X-ray photoelectron spectra (XPS) were obtained using a Thermo Scientific K-Alpha meter with Al Kα radiation as the X-ray source. The binding energy was calibrated against the C 1s peak at 284.8 ± 0.2 eV.

2.2.3. Microbial analysis

High-throughput 16S rRNA gene sequencing was used to analyse the bacterial community in different groups. Microbial samples were taken from the initial inoculum before fermentation and the effluents after the fermentation of *L. digitata* (as a representative group). The DNA extraction and sequencing procedures to identify the bacteria community were performed by Shanghai Majorbio Bio-pharm Technology Co., Ltd (Shanghai, China). The methods for sample preparation and microbial analysis were detailed in a previous study [36]. The raw sequence data were deposited into the Sequence Read Archive database of the National Centre for Biotechnology Information with a BioProject accession code of PRJNA742045. The sequence data were analysed on the Majorbio Cloud Platform (www.majorbio.com) using RDP Classifier with reference to the silva 138/16s_bacteria database.

2.2.4. Kinetic modelling

The kinetic parameters for the fermentation process were calculated by fitting the modified Gompertz Equation (Eq. (2)). The peak fermentation time was defined as per Eq. (3).

$$H = H_m \times \exp\left\{ -\exp\left[\frac{R_m e}{H_m}(\lambda - t) + 1\right]\right\} \quad \text{(Eq. 2)}$$

$$T_m = \frac{H_m}{R_m e} + \lambda \quad \text{(Eq. 3)}$$

where H_m is the maximum biohydrogen yield, R_m is the peak production rate, λ is the lag-phase time, and T_m is the peak fermentation time.

3. Results and discussion

3.1. Physical and chemical properties of carbon materials

The elemental composition of each carbon material is shown in Table 3. Graphene had the highest carbon content and lowest hydrogen and nitrogen content. Wood_Biochar had the second-highest carbon content and the second-lowest nitrogen content. The two draff-derived biochars (namely Draff_N_2_Biochar and Draff_CO_2_Biochar) had similar carbon, hydrogen, and nitrogen content. The higher nitrogen content of Draff_N_2_Biochar and Draff_CO_2_Biochar was attributed to the higher protein content in the draff feedstock for pyrolysis [37]. Draff_CO_2_Biochar had the highest oxygen content of 9.2% as the purge gas CO_2 could also act as an activation agent during the pyrolysis to modify the surface functional groups and increase the abundance of oxygen [38].

The surface properties of the carbon materials are shown in Table 4. The specific surface area of graphene was the highest. Wood_Biochar and Draff_CO_2_Biochar had lower specific surface areas compared to graphene and Draff_N_2_Biochar. The pH value of graphene suspension was the lowest indicating the existence of acidic functional groups. The two draff-derived biochars were close to pH neutral. Wood_Biochar had the highest pH value of 9.09. The EC of the materials significantly varied in a wide range. The EC of graphene was the highest, which was two orders of magnitude larger than the EC of Draff_CO_2_Biochar and three orders of magnitude larger than the EC of Draff_N_2_Biochar and Wood_Biochar.

Fig. 1 shows the FTIR spectra of the carbon materials for a qualitative analysis of the surface functional groups. The absorbance peak at the wavenumber around 3400 cm^{-1} indicated the existence of O—H [39]. The absorbance peak at 2930 cm^{-1} indicated the existence of aliphatic C—H [40]. The peak at 1640 cm^{-1} was due to the quinone/ketone C═O [41], which was observed on graphene and Wood_Biochar samples but not observed on Draff_N_2_Biochar and Draff_CO_2_Biochar. The peak at 1570 cm^{-1} was due to the stretching vibration of aromatic C═C [41]. The peak at 1120 cm^{-1} was attributed to the stretching vibration of C—O [40]. The C—O peaks on graphene and Wood_Biochar were mild whereas those on Draff_N_2_Biochar and Draff_CO_2_Biochar were sharp.

Fig. S1 in the supplementary material shows the XPS spectra of carbon (XPS region: C1s) on the surface of the carbon materials. The C1s spectra were deconvoluted into six peaks, each of which represented a functional group. The peaks centred at the binding energy of 284.4 eV, 284.8 eV, 285.7 eV, 287.0 eV, 288.9 eV, and 290.4 eV were attributed to the sp^2 hybridised carbon (such as graphitic/aromatic carbon), sp^3 hybridised carbon (such as hydrocarbon), —C—O group (such as alcohol/ether), —C═O group (such as quinone/ketone), —COOR group (such as carboxyl/ester), and the π-π* shake-up satellite peak (satellite of graphitic carbon), respectively [42–44]. The integral peak area indicated the relative abundance of each functional group. Normalization was conducted on the integral area of the peaks and the results are shown in Table 5. The predominant peak at 284.4 eV observed on graphene was due to the sp^2 hybridised carbon, which is also the C1s peak for graphite as determined from the XPS of single crystal graphite [42,44]. A clear π-π* satellite was seen 6 eV away from the sp^2 C peak of graphene. These two peaks indicated the predominance of the conjugated π-electron systems in graphene, which contributed to the high electrical conductivity of graphene. The remaining carbon species on graphene was the —C═O group, which might be formed due to the oxidation of graphene during the storage and testing processes. Wood_Biochar had the second-highest abundance of sp^2 hybridised carbon, only 8% lower than that of graphene. It was inferred that graphitic/aromatic carbon structure was the dominant carbon structure on Wood_Biochar. However, no π-π* shake-up satellite peak was observed on Wood_Biochar. The

Table 3
Compositional characteristics of the carbon materials.

Sample name	Elemental composition (%TS)				Ash (% TS)	Molar ratio	
	C	H	N	O		O/C	H/C
Graphene	91.7 ± 0.0	0.6 ± 0.0	0.1 ± 0.1	7.6 ± 0.0	\	0.06	0.08
Draff_N_2_Biochar	72.2 ± 0.5	1.1 ± 0.0	5.5 ± 0.1	6.7 ± 0.4	14.5 ± 0.3	0.07	0.18
Draff_CO_2_Biochar	71.8 ± 1.6	1.2 ± 0.0	5.2 ± 0.1	9.2 ± 1.0	12.6 ± 0.1	0.10	0.20
Wood_Biochar	87.8 ± 0.3	2.1 ± 0.0	0.7 ± 0.0	7.0 ± 0.2	2.4 ± 0.1	0.06	0.29

Table 4
Surface area, porosity, pH, and EC of the carbon materials.

Sample name	S_{BET} (m^2/g)	V_{total} (m^3/g)	V_{micro} (cm^3/g)	Avg. pore width (nm)	pH	EC (mS/m)
Graphene	500.0[a]	\	\	\	4.75 ± 0.38	11021.0 ± 3444.0
Draff_N_2_Biochar	227.8	0.126	0.102	2.207	7.12 ± 0.02	23.8 ± 0.4
Draff_CO_2_Biochar	135.2	0.076	0.062	2.249	7.74 ± 0.22	200.0 ± 33.0
Wood_Biochar	161.5	0.101	0.070	2.493	9.09 ± 0.14	86.5 ± 35.0

Note: S_{BET} = Specific Surface Area, V_{total} = Volume of total pores, V_{micro} = Volume of micropores, EC = Electrical Conductivity.
[a] Data from the product description of Sigma Aldrich.

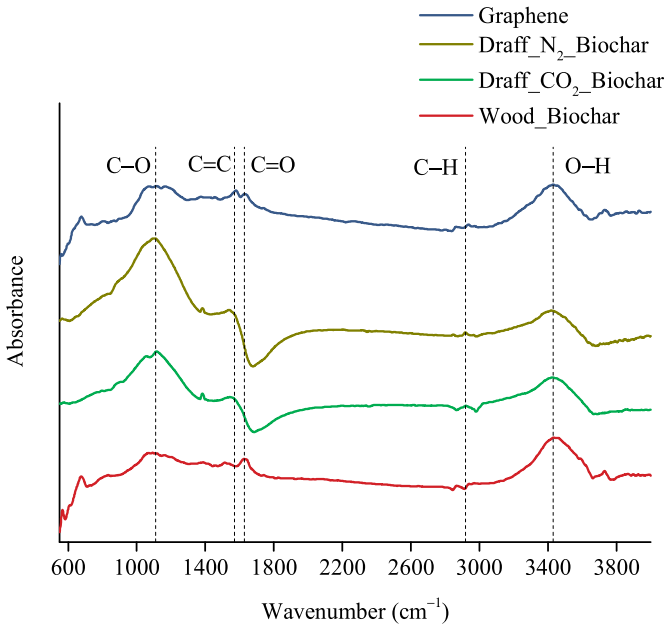


Fig. 1. The FTIR spectra of different carbon materials.

abundance of total oxygen-containing functional groups (namely −C−O, −C═O, and −COOR) on Wood_Biochar was 20.9%, which was lower than Draff_N_2_Biochar (35.7%) and Draff_CO_2_Biochar (31.6%). Draff_N_2_Biochar and Draff_CO_2_Biochar had a lower abundance of sp^2 carbon and a higher abundance of sp^3 carbon compared to Wood_Biochar, indicating the lower graphitisation/aromatisation degree of the two draff-derived biochars.

Fig. S2 in the supplementary material shows the deconvolution of nitrogen (XPS region: N1s) spectra into three peaks: pyridinic-N at 398.1 eV, pyrrolic-N at 400.0 eV, and graphitic-N at 401.5 eV [45]. The normalized results are shown in Table 6. Pyrrolic-N and graphitic-N were the predominant groups on graphene and Wood_Biochar. The abundance of pyrrolic-N was close to the abundance of graphitic-N on both graphene and Wood_Biochar. It must be noted that the total nitrogen content in graphene and Wood_Biochar were both less than 1%. In contrast, the total nitrogen content in Draff_N_2_Biochar and Draff_CO_2_Biochar were both higher than 5%. The predominant nitrogen-containing groups on both Draff_N_2_Biochar and Draff_CO_2_Biochar were pyrrolic-N and pyridinic-N. Both pyridinic-N and graphitic-N can enhance the electrical conductivity of carbon materials by donating electrons to the conductive π-system [46].

Table 6
Relative abundance of different nitrogen-containing functional groups.

N species	Pyridinic-N	Pyrrolic-N	Graphitic-N
Sample	398.1 eV	400.0 eV	401.5 eV
Graphene	0	53.6%	46.4%
Draff_N_2_Biochar	35.4%	41.6%	23.0%
Draff_CO_2_Biochar	40.5%	56.0%	3.4%
Wood_Biochar	0	49.7%	50.3%

Note: The relative abundance of each functional group was determined by the integral area of its characteristic peak in the X-ray photoelectron spectra.

3.2. Hydrogen and VFA production from glucose

Two major metabolic pathways for biohydrogen production from glucose can be expressed as R1 and R2, namely the acetic acid pathway and the butyric acid pathway, respectively. The maximum biohydrogen potential of glucose calculated as per R1 and R2 was 498 and 249 ml/g, respectively.

$$C_6H_{12}O_6 + 2H_2O \rightarrow 2CH_3COOH + 2CO_2 + 4H_2 \quad (R1)$$

$$C_6H_{12}O_6 \rightarrow CH_3CH_2\,CH_2COOH + 2CO_2 + 2H_2 \quad (R2)$$

Fig. 2 (a) shows the cumulative biohydrogen yield from glucose with the addition of different carbon materials at the same concentration of 1 g/L. In the control group without carbon additives, the biohydrogen yield from glucose was 67.9 ± 5.2 ml/g, which was within the range found for thermophilic temperatures in literature (55−174 ml/g) [47,48]. The variation in biohydrogen production from glucose was attributed to the changes in the fermentation temperature, pH, reactor configuration, and inoculum activity in different studies. The optimal C/N ratio for fermentation was suggested to be 20−30 [49]. The relatively low hydrogen yield from glucose in this study might be attributed to the limited nitrogen supply for the basic metabolisms of the fermentation bacteria as no nitrogen sources were added in the feedstock. The addition of

Table 5
Relative abundance of different carbon functional groups.

C species	sp^2 C	sp^3 C	−C−O	−C═O	−COOR	π-π* shake-up satellite
Sample	284.4 eV	284.8 eV	285.7 eV	287.0 eV	287.8 eV	290.4 eV
Graphene	73.5%	0	0	16.6%	0	9.9%
Draff_N_2_Biochar	19.2%	39.0%	24.4%	6.5%	4.8%	6.1%
Draff_CO_2_Biochar	32.4%	34.9%	23.5%	3.4%	4.7%	1.1%
Wood_Biochar	67.3%	11.9%	10.3%	1.9%	8.7%	0%

Note: The relative abundance of each functional group was determined by the integral area of the characteristic peak in the X-ray photoelectron spectra.

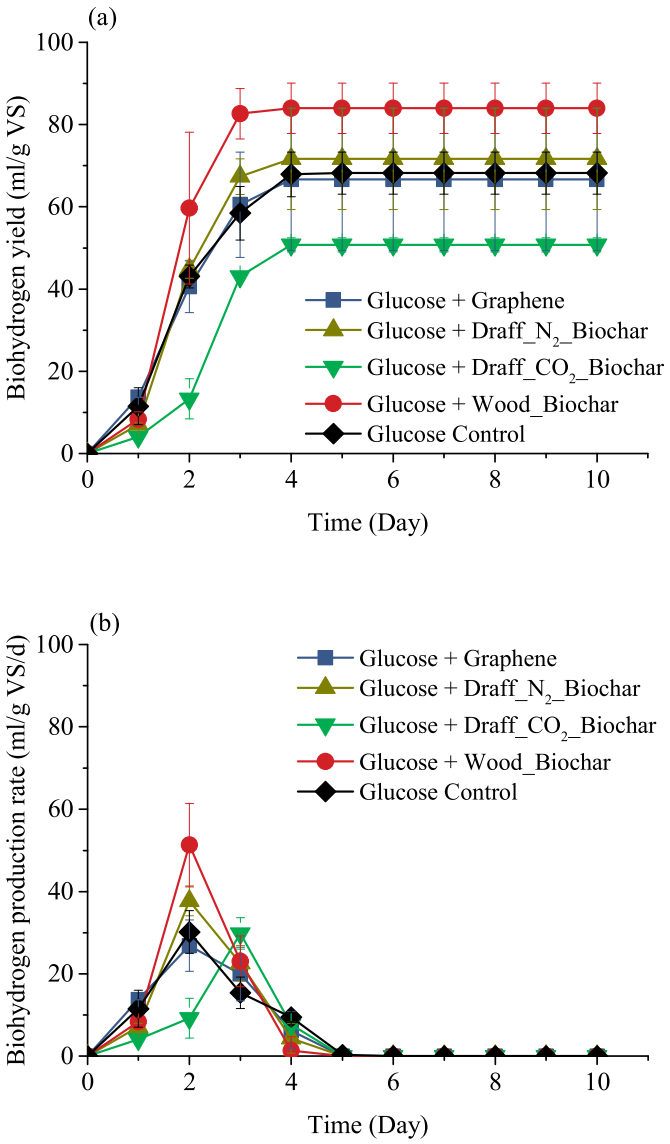


Fig. 2. (a) Cumulative biohydrogen yield from glucose affected by different carbon materials; (b) Biohydrogen production rate from glucose affected by different carbon materials.

graphene, Draff_N_2_Biochar, and Draff_CO_2_Biochar did not lead to significant ($p > 0.05$) impacts on the hydrogen yield from glucose. The addition of Wood_Biochar insignificantly ($p > 0.05$) increased biohydrogen yield.

Fig. 2 (b) shows the biohydrogen production rate from glucose. The addition of graphene, Draff_N_2_Biochar, and Draff_CO_2_Biochar led to no significant ($p > 0.05$) changes in the peak production rate. The addition of Wood_Biochar significantly ($p < 0.05$) increased the peak production rate by 70% in contrast to the control group. The kinetic parameters for the fermentation of glucose (Table 7) were obtained by fitting the modified Gompertz model (Eq. (2)). The predicted maximum biohydrogen yield (H_m) exhibited a good fit with the BHP results with R^2 (the coefficients of determination) between 0.995 and 0.999. However, there was a significant difference (9%–33%) between the predicted and measured peak production rate. The relatively low coincidence was potentially ascribed to the small number of data samples for the model fitting. As shown in Table 7, the addition of the four carbon materials did not reduce the lag-phase time. This might be attributed to the short lag-phase time for glucose fermentation as glucose was a readily digestible feedstock for the bacteria.

Fig. 3 shows the production of VFAs in glucose fermentation. The major VFAs consisted of acetic acid, iso-butyric acid, and butyric acid. In the control group G5 in the absence of carbon materials, an amount of 948 mg/L VFAs was produced within Day 1. The concentration of acetic acid did not significantly increase from Day 1 to Day 6, while the concentration of butyric acid increased by 101%. This observation suggested that the butyric acid pathway was the predominant pathway in G5. The estimated corresponding H_2 yield in G5 from acetic and butyric acid (as per R1 and R2) was 42.6 ml/g. The actual H_2 yield in G5 was 67.9 ml/g, suggesting that H_2 was also formed through other metabolic pathways such as the formic acid pathway [50,51]. The addition of graphene (G1), Draff_N_2_Biochar (G2), Draff_CO_2_Biochar (G3) and Wood_Biochar (G4) increased the final production of VFAs by 75%, 63%, 28%, and 29%, respectively. The increases in VFA production were not accompanied by significant increases in biohydrogen production. A possible reason was that the hydrogen consuming reactions were promoted simultaneously, such as the homoacetogenic reaction as per R3.

$$4H_2 + 2CO_2 \rightarrow CH_3COOH + 2H_2O \quad (R3)$$

3.3. Hydrogen and VFAs production from cellulose

Fig. 4 (a) shows the cumulative biohydrogen production from cellulose. The biohydrogen yield was in the range of 15.4–19.5 ml/g cellulose in all the experimental groups. At thermophilic temperature, Xia et al. obtained a biohydrogen yield of 5 ml/g cellulose [52]. Cellulose is made up of β (1 → 4) linked glucose units, tightly packed via hydrogen bonds. It is highly resistant to deconstruction by hydrogen-producing bacteria. The fibrillar compartment in the cell wall of algae formed mainly of cellulose was considered the major factor that hinders the biohydrogen production from algae species [17,53]. As shown in Fig. 4, the addition of different carbon materials did not significantly ($p > 0.05$) change the biohydrogen yield or the peak production rate in comparison with the control group.

The kinetic parameters for cellulose fermentation are shown in Table 8. There was a difference between the predicted and the measured peak production rate with distinct R^2. Nonetheless, the kinetic parameters in Table 8 suggested that the addition of carbon materials did not significantly change the lag-phase time and the peak fermentation time for cellulose fermentation. Notably, the low biohydrogen yields were potentially due to the inefficiency of the cellulolytic enzyme activity, which is responsible for hydrolysis of cellulose to easily fermentable glucose. Zhao et al. found that cornstalk derived biochar had no effect on the cellulase activity and did not promote the saccharification of lignocellulose by the external cellulase [54].

Considering the low biohydrogen production from cellulose, the VFAs production from cellulose was also reasonably low as shown in Fig. 5. In the control group G10, no detectable acetic acid was observed during fermentation. On Day 1, the addition of graphene (G6) and Wood_Biochar (G9) enhanced the yield of acetic acid to 72–73 mg/L. From Day 2 to Day 4, the addition of graphene increased the accumulation of butyric acid by 133% compared with G10, whilst the addition of Draff_N_2_Biochar, Draff_CO_2_Biochar, and Wood_Biochar did not significantly impact the final production of butyric acid. However, in the graphene and Wood_Biochar amended groups, the acetic acid was reduced over the fermentation process. The consumption of acetic acid might take place through the reaction R4 [50]:

Table 7
Kinetic parameters for the fermentation of glucose with different carbon materials.

Group	Experimental results		Kinetic model parameters				
	BHP (ml/g VS)	P (ml/g VS/d)	H_m (ml/g VS)	R_m (ml/g VS/d)	λ (d)	T_m (d)	R^2
Glucose + Graphene	66.7 ± 17.4	26.9 ± 6.2	67.2 ± 0.5	31.6 ± 1.5	0.6 ± 0.1	1.4 ± 0.0	0.998
Glucose + Draff_N_2_Biochar	71.7 ± 12.3	37.7 ± 3.6	72.0 ± 0.3	44.1 ± 1.3	0.9 ± 0.0	1.5 ± 0.0	0.999
Glucose + Draff_CO_2_Biochar	50.8 ± 1.7	29.8 ± 6.5	50.9 ± 0.6	39.7 ± 4.3	1.7 ± 0.1	2.1 ± 0.0	0.995
Glucose + Wood_Biochar	84.6 ± 6.1	51.3 ± 2.0	84.8 ± 1.0	60.6 ± 3.9	0.9 ± 0.1	1.4 ± 0.1	0.999
Glucose Control	67.9 ± 5.2	30.1 ± 7.2	68.5 ± 0.4	32.9 ± 1.3	0.7 ± 0.0	1.4 ± 0.0	0.999

Note: BHP = biohydrogen yield in the biohydrogen potential assay, P = peak production rate in the biohydrogen potential assay, H_m = maximum biohydrogen yield, R_m = peak biohydrogen production rate, λ = lag-phase time, and T_m = peak fermentation time.

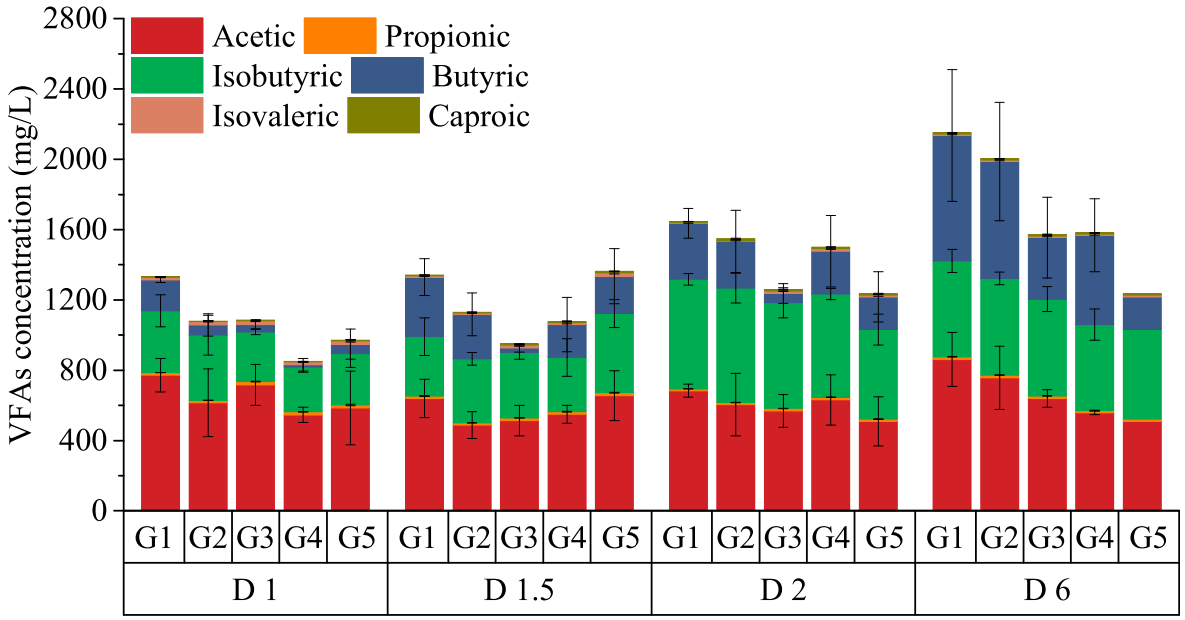


Fig. 3. Concentration of VFAs produced in the fermentation of glucose with different carbon materials. Note: G = Group, D = Day. G1: Glucose + Graphene; G2: Glucose + Draff_N_2_Biochar; G3: Glucose + Draff_CO_2_Biochar; G4: Glucose + Wood_Biochar; G5: Glucose Control.

$2CH_3COOH + 2H_2 \rightarrow CH_3CH_2CH_2COOH + 2H_2O$ (R4).

3.4. Hydrogen and VFAs production from L. digitata

The biohydrogen yield from *L. digitata* is shown in Fig. 6 (a). Seaweed polysaccharides are more complex when compared to glucose and cellulose. Therefore, the bacteria took a longer time to acclimatise and start to break down the cell walls of *L. digitata*. The yield in the control group was 40.6 ml/g VS. Wet L. *digitata* was used in this study and it was expected to be less degradable than dried *L. digitata* due to the intact cell wall of the wet *L. digitata* [55]. The addition of the four carbon materials did not significantly ($p > 0.05$) change the biohydrogen yield. Fig. 6 (b) shows the biohydrogen production rate. From a perspective of statistics, the addition of the four carbon materials did not change the peak production rate significantly ($p > 0.05$) due to the large deviations between the triple values in the control group. However, all the carbon materials significantly ($p < 0.05$) reduced the lag-phase time and antedated the production peak. The kinetic parameters for the fermentation of *L. digitata* are shown in Table 9. The predicted maximum biohydrogen yield (H_m) exhibited a good fit with the measured data. A significant difference (2%–38%) between the predicted and the measured peak production rate was observed with distinct R^2. As compared with the control group, the lag-phase time was reduced by 47%, 36%, 37%, and 49% by graphene, Draff_N_2_Biochar, Draff_CO_2_Biochar, and Wood_Biochar, respectively. The peak fermentation time was reduced by 44%, 31%, 39%, and 45% by graphene, Draff_N_2_Biochar, Draff_CO_2_Biochar, and Wood_Biochar, respectively. Generally, the two draff-derived biochars Draff_N_2_Biochar and Draff_CO_2_Biochar were less effective than graphene and Wood_Biochar in terms of reducing lag-phase time and accelerating the fermentation. Draff_CO_2_Biochar led to slightly better performance with shorter lag-phase time and peak fermentation time as compared to Draff_N_2_Biochar.

The production of VFAs in the fermentation of *L. digitata* is shown in Fig. 7. During the lag phase (the first three days), a small amount of VFAs was produced. It was inferred that these VFAs were produced from the readily digestible component exposed during the physically mincing of wet *L. digitata*. From Day 4 to Day 10, the VFAs accumulated gradually. In the control group G15, the final concentration of total VFAs was 932 mg/L. The final concentration of VFAs in the graphene amended group G11 was 53% higher than that in G15. In the Draff_N_2_Biochar amended group G12 and the Draff_CO_2_Biochar amended group G13, the final concentration of VFAs was slightly lower than that in G15. The Wood_Biochar amended group G14 accumulated a 6% higher amount of VFAs compared to G15 on Day 10.

The molar ratio of acetate/butyrate in G15 was 0.84, close to the value of ca. 0.8 in a continuous hydrolysis reactor treating *L. digitata* at mesophilic temperature [9]. The addition of graphene,

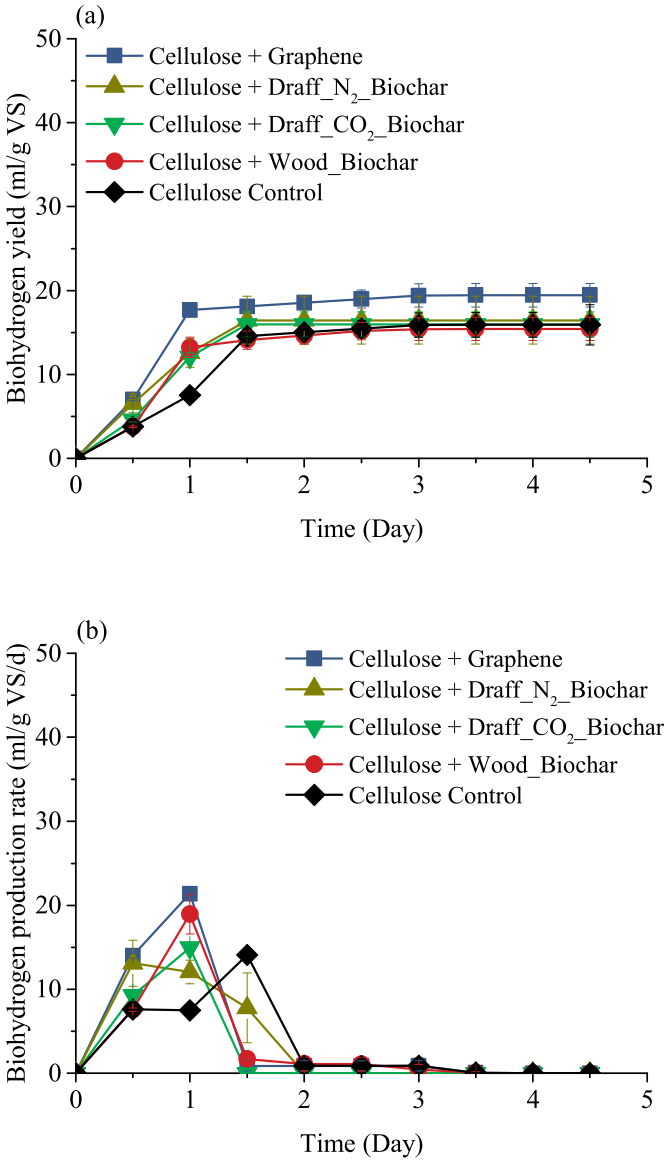


Fig. 4. (a) Cumulative biohydrogen yield from cellulose affected by different carbon materials; (b) Biohydrogen production rate from cellulose affected by different carbon materials.

Draff_CO_2_Biochar, and Wood_Biochar increased the acetate/butyrate ratio to 1.57, 1.10, and 0.89, respectively. The addition of Draff_N_2_Biochar slightly decreased the acetate/butyrate ratio to 0.78. There are arguments over the relationship between the biohydrogen yield and the acetate/butyrate ratio. Some studies concluded that higher biohydrogen yields were associated with higher acetate/butyrate ratios [56]. However, some studies had a contrasting conclusion [57]. This might be ascribed to the complex metabolic network in fermentation, as different pathways could lead to the production of acetic acid and butyric acid either with or without biohydrogen production. The addition of graphene significantly facilitated the production of acetic acid. A similar phenomenon was observed in the thermophilic fermentation of glucose, in which activated carbon facilitated the production of acetic acid rather than butyric acid and ethanol [57]. Graphene increased the overall production of VFAs but did not significantly increase the production of biohydrogen. The following may describe the reasons: (1) Graphene as an electron conductor between acid-producers and homoacetogens may simultaneously have enhanced homoacetogenesis, which may have converted biohydrogen and CO_2 into acetic acid [58]; (2) High levels of acetic and butyric acids may have been produced through other non-hydrogenogenic pathways such as mediated by heterotrophic/autotrophic homoacetogenes. The fermentation process was dominated by several overlapping and competing fermentation pathways, which might reduce the biohydrogen yield in comparison to the relatively high yield of VFAs [59,60].

3.5. Bacteria community affected by carbon materials

Fig. 8 shows the microbial community in the fermentation of *L. digitata* with different additives. At the phylum level, the bacteria community in the inoculum consisted of *Firmicutes* (8.7%) and *Proteobacteria* (91.3%). The control group G15 consisted of primarily *Firmicutes* (97.3%), *Proteobacteria* (1.4%), *Actinobacteria* (1.0%), and other phyla with relative abundance less than 1%. *Firmicutes* included the main hydrogen-producing microbes, which could utilize a wide range of substrates [61]. In the graphene amended group G11, the predominant phyla were *Firmicutes* (97.6%). *Firmicutes* were also the predominant phyla in Draff_N_2_Biochar amended group G12 and Draff_CO_2_Biochar amended group G13. In the Wood_Biochar amended group G14, the major phyla included *Firmicutes* (95.1%), *Proteobacteria* (2.1%), *Actinobacteria* (1.6%). *Proteobacteria* were the most abundant bacteria in bioreactors treating high concentration wastewaters [62]. *Actinobacteria* were reported as the major drivers of hydrolysis and acidification [59,62].

At the genus level, the predominant genera in the inoculum were *Pseudomonas* (91.2%) and *Clostridium sensu stricto 7* (6.5%). *Pseudomonas* contained heterotrophic bacteria species which were unbeneficial to hydrogen production. The predominant genera in the control group included *Thermoanaerobacterium* (24.6%), *Bacillus* (65.8%), *Clostridium sensu stricto 7* (3.4%), and *Syntrophaceticus* (1.6%). *Thermoanaerobacterium* and *Bacillus* were significantly enriched. *Thermoanaerobacterium* grew rapidly at 55–70 °C and all of the known *Thermoanaerobacterium* species were reported to possess hydrolase benefiting fermentative hydrogen production.

Table 8
Kinetic parameters for the fermentation of cellulose with different carbon materials.

Group	Experimental results		Kinetic model parameters				
	BHP (ml/g VS)	P (ml/g VS/d)	H_m (ml/g VS)	R_m (ml/g VS/d)	λ (d)	T_m (d)	R^2
Cellulose + Graphene	19.5 ± 1.4	21.4 ± 0.3	20.0 ± 0.3	29.5 ± 4.3	0.3 ± 0.0	0.5 ± 0.0	0.993
Cellulose + Draff_N_2_Biochar	16.5 ± 0.3	13.2 ± 2.7	14.5 ± 0.6	18.4 ± 0.9	0.1 ± 0.0	0.4 ± 0.0	0.999
Cellulose + Draff_CO_2_Biochar	16.0 ± 1.5	15.0 ± 0.5	16.1 ± 0.1	19.0 ± 1.2	0.3 ± 0.0	0.6 ± 0.0	0.998
Cellulose + Wood_Biochar	15.4 ± 1.4	18.9 ± 2.4	15.2 ± 0.2	24.6 ± 2.6	0.3 ± 0.0	0.6 ± 0.0	0.994
Cellulose Control	15.9 ± 2.4	14.1 ± 0.8	16.1 ± 0.5	12.4 ± 1.9	0.3 ± 0.1	0.7 ± 0.0	0.978

Note: BHP = biohydrogen yield in the biohydrogen potential assay, P = peak production rate in the biohydrogen potential assay, H_m = maximum biohydrogen yield, R_m = peak biohydrogen production rate, λ = lag-phase time, and T_m = peak fermentation time.

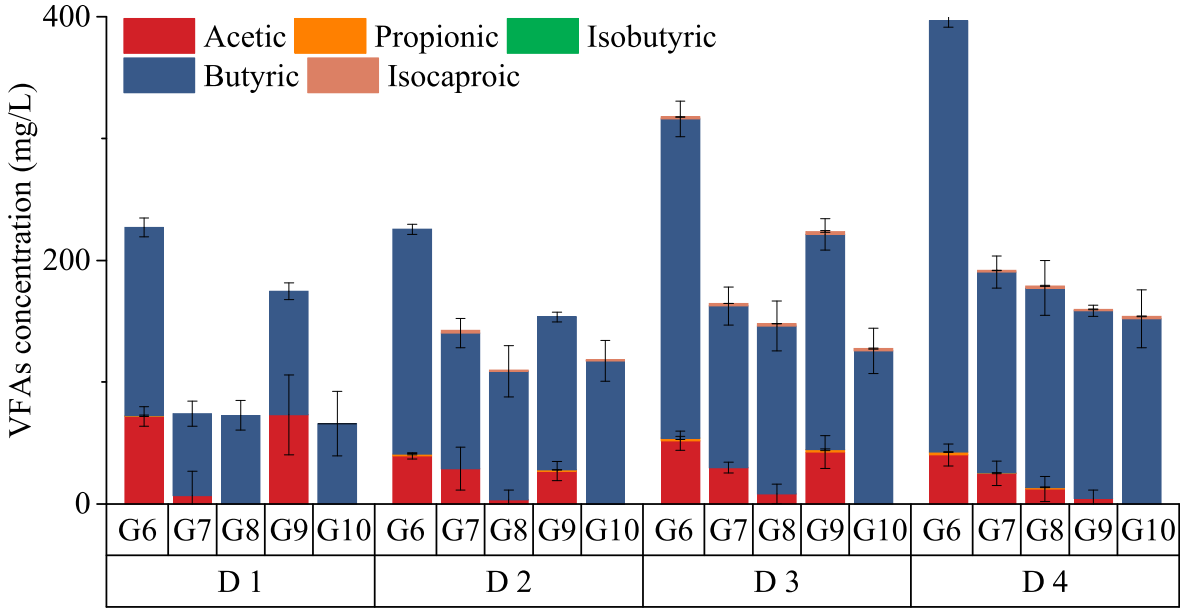


Fig. 5. Concentration of VFAs produced in the fermentation of cellulose with different carbon materials. Note: G = Group, D = Day. G6: Cellulose + Graphene; G7: Cellulose + Draff_N_2_Biochar; G8: Cellulose + Draff_CO_2_Biochar; G9: Cellulose + Wood_Biochar; G10: Cellulose Control.

Some *Thermoanaerobacterium* species (for example, the *T. thermosaccharolyticum*) were identified as efficient hydrogen producers, even more efficient as compared to *Clostridium* and *Enterobacter* species [63]. Jia et al. observed that the abundance of *Thermoanaerobacterium* positively correlated with hydrogen production rate [64]. The addition of graphene, Draff_N_2_Biochar, Draff_CO_2_Biochar, and Wood_Biochar increased the relative abundance of *Thermoanaerobacterium* to 90.4%, 55.6%, 31.9%, and 80.1%, respectively. This might be responsible for the accelerated biohydrogen production with the addition of these carbon materials. The addition of Wood_Biochar slightly increased the abundance of *Clostridium sensu stricto 7* (3.9%) compared to the control group. *Clostridium sensu stricto 7* is a typical hydrogen-producing genus identified in thermophilic fermentation [51]. Almost all *Clostridium sensu stricto* strains produce butyrate as the main metabolic product, not excluding the production of various organic acids and alcohols (such as formic acid and ethanol) [65,66]. Althuri and Mohan demonstrated that some species of *Clostridium sensu strict 7* could use carbon sources such as glucose and cellulose to produce ethanol [67]. The enrichment of *Clostridium sensu stricto 7* was also observed in the fermentation with the addition of activated carbon or transition elements such as Fe and Ni [51,58]. In comparison to the control group, the addition of graphene, Draff_N_2_Biochar, and Wood_Biochar decreased the relative abundance of *Bacillus*. *Bacillus* include many species that have diverse metabolic activities. Some of *Bacillus* species were able to produce biohydrogen [8].

3.6. Proposed role of carbon materials in facilitating fermentation of *L. digitata*

Table 10 summarises the reported studies investigating the effects of carbon materials (including biochar, activated carbon, and carbon cloth) on biohydrogen fermentation. The positive effects of different carbon additives included improving the yield of biohydrogen and VFAs, accelerating production rate, and reducing lag-phase time. In this study, the carbon additives did not statistically increase the biohydrogen yield from *L. digitata*, but an increase of 53% in the VFA yield was observed with the addition of graphene. Porous carbon materials could support the formation of biofilm to increase microbial density, mitigate the inhibitory accumulation of soluble metabolites, and increase the dehydrogenase activity [30,68,69]. It was also observed that algae cell walls were physically disrupted in the presence of biochar, which increased the availability of macromolecular organic substrates for further hydrolysis during the fermentation of algae [70]. Moreover, conductive carbon materials were found to promote the potential bacterial electron transfer [28,31], which facilitated microbial metabolic activities.

The physicochemical properties of the carbon materials were the major factors in determining their functions in the fermentation process. The fermentation performance of *L. digitata* was evaluated in terms of the biohydrogen yield, peak production rate, acetic acid production, total VFAs production, and lag-phase time. The properties of the carbon materials were determined in terms of the total carbon and nitrogen content, molar O/C and H/C ratios, the relative abundance of each surface functional group (such as the carbon species, oxygen-containing groups, and nitrogen-containing groups), the specific surface area, and the EC. Mathematic correlations between the enhanced fermentation performance and the key properties of the carbon materials were analysed to establish relationships between them. As the variations in biohydrogen yield and peak production rate among different fermentation groups were statistically insignificant, the biohydrogen yield and peak production rate were excluded from the correlation assessment.

As shown in Fig. 9 (a), the acetic acid production and the total VFA production were positively correlated to the EC of carbon materials and the slopes were significantly different from zero at the $p = 0.05$ level. The lag-phase time was negatively correlated to the total carbon content and the relative abundance of sp^2 carbon as shown in Fig. 9 (b) and (c), but positively related to the abundance of total oxygen-containing functional groups as shown in Fig. 9 (d). The positive effects of promoting the acetic acid and VFAs production and reducing the lag-phase time were postulated as being associated with the high EC, high carbon content, high abundance of sp^2 carbon, and low abundance of oxygen-containing

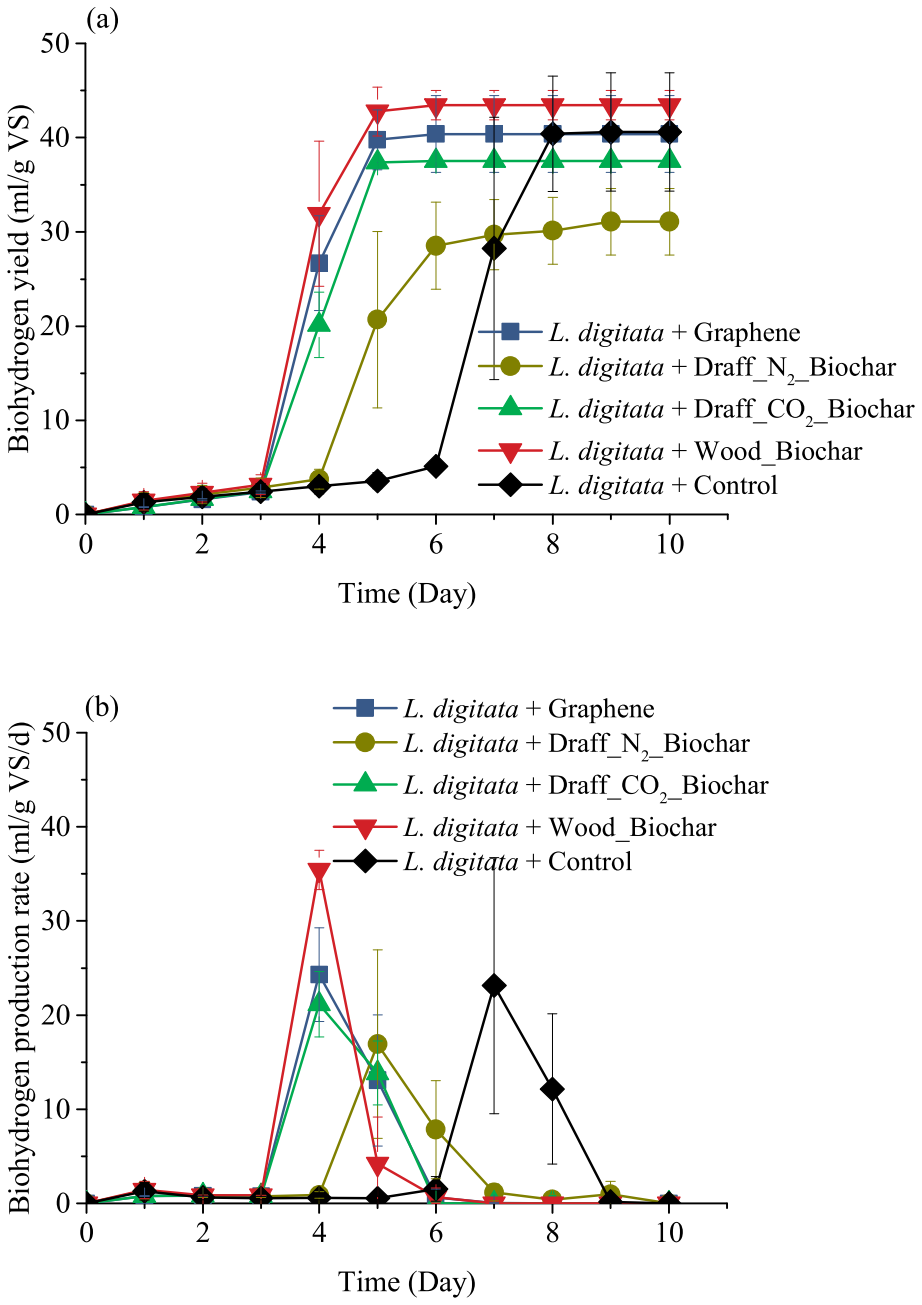


Fig. 6. (a) Cumulative biohydrogen yield from *L. digitata* affected by different carbon additives; (b) Biohydrogen production rate from *L. digitata* affected by different carbon additives.

Table 9
Kinetic parameters for the fermentation of *L. digitata* with different carbon additives.

Group	Experimental results		Kinetic model parameters				
	BHP (ml/g VS)	P (ml/g VS/d)	H_m (ml/g VS)	R_m (ml/g VS/d)	λ (d)	T_m (d)	R^2
L. digitata + Graphene	40.4 ± 5.0	24.3 ± 4.9	40.7 ± 0.4	30.2 ± 2.2	3.1 ± 0.7	3.6 ± 0.0	0.998
L. digitata + Draff_N_2_Biochar	31.1 ± 4.3	22.7 ± 7.0	30.7 ± 0.7	18.8 ± 2.5	3.8 ± 0.1	4.4 ± 0.1	0.991
L. digitata + Draff_CO_2_Biochar	37.5 ± 0.1	21.2 ± 3.4	37.8 ± 0.5	27.4 ± 2.9	3.1 ± 0.1	3.6 ± 0.1	0.996
L. digitata + Wood_Biochar	43.4 ± 3.1	35.4 ± 2.6	43.6 ± 0.6	34.8 ± 3.2	3.0 ± 0.1	3.5 ± 0.1	0.996
L. digitata Control	40.6 ± 7.7	23.1 ± 0.6	41.3 ± 1.5	27.2 ± 4.4	5.9 ± 0.1	6.4 ± 0.1	0.986

Note: BHP = biohydrogen yield in the biohydrogen potential assay, P = peak production rate in the biohydrogen potential assay, H_m = maximum biohydrogen yield, R_m = peak biohydrogen production rate, λ = lag-phase time, and T_m = peak fermentation time of the fermentation process.

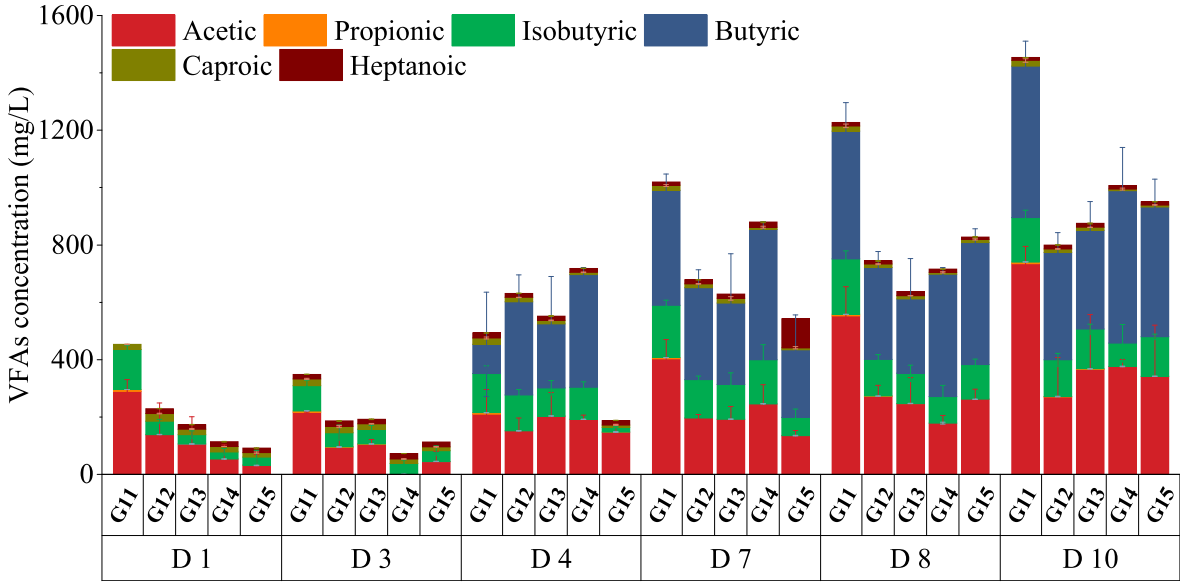


Fig. 7. Concentration of VFAs produced in the fermentation of *L. digitata* with different carbon materials. Note: G = Group, D = Day. G11: *L. digitata* + Graphene; G12: *L. digitata* + Draff_N_2_Biochar; G13: *L. digitata* + Draff_CO_2_Biochar; G14: *L. digitata* + Wood_Biochar; G15: *L. digitata* Control.

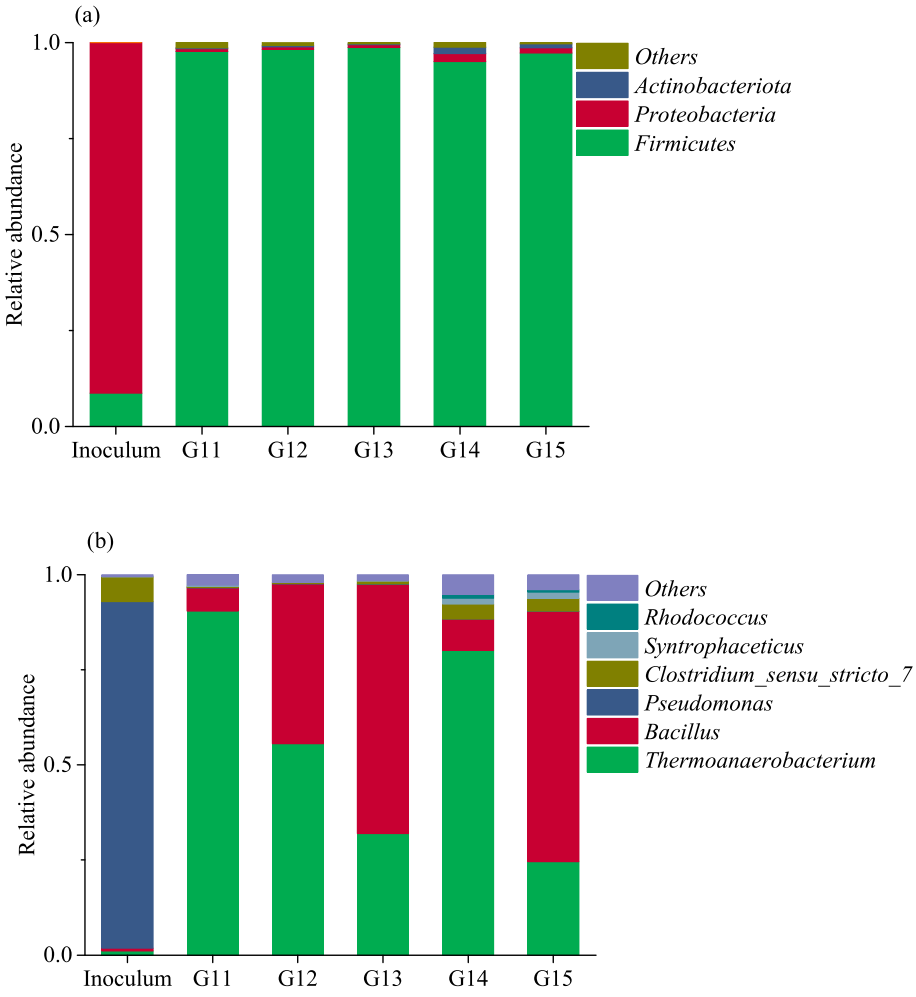


Fig. 8. Bacteria community in the fermentation of *L. digitata* with the addition of different carbon materials at (a) phylum and (b) genus level. Note: G = Group. G11: *L. digitata* + Graphene; G12: *L. digitata* + Draff_N_2_Biochar; G13: *L. digitata* + Draff_CO_2_Biochar; G14: *L. digitata* + Wood_Biochar; G15: *L. digitata* Control.

Table 10
A summary of studies focusing on the effects of different carbon materials on fermentative biohydrogen production.

Feedstock	Carbon material	Pyrolysis temperature (°C)	Addition dosage (g/L)	Fermentation temperature (°C)	Inoculum	H_2/VFAs yield	Production rate	Proposed role of carbon materials	Reference
Glucose	Carbon cloth		1.0		*Enterobacter aerogenes*	H_2 +26.6%	Peak rate +60%	Supporting the attachment of bacteria; promoting bacterial electron transfer	[28]
Glucose	Corn-bran residue biochar	600	0.6	37	Sewage sludge heated at 85 °C	H_2 +29%	Peak rate +20%; Lag phase −40%	Promoting the biofilm formation; maintaining suitable pH	[29]
Glucose	Rice straw biochar	500	10	37	*Clostridium beijerinckii*	H_2 +49%		Regulating reducing power; accelerating re-assimilation of acids	[30]
Glucose	Rice husk biochar	550	0.6	36	Granular sludge	Acetate +32%		Facilitating syntrophic growth of fermentative bacteria and homoacetogens in the biofilm	[31]
	Wood biochar					Acetate +38%			
	Longan shell biochar					Acetate +72%			
	Corncob biochar					Acetate +12%			
	White popine biochar					Acetate +32%			
	Pinecone biochar					Acetate −2%			
	Bagasse biochar					Acetate +40%			
	Bamboo biochar					Acetate +46%			
	Coconut biochar					Acetate +110%			
	Activated carbon					Acetate +69%			
Glucose	Graphene		1.0	55	Sludge heated at 100 °C	VFAs +75%		Supporting biofilm development; enhancing bacterial electron transfer	This study
	Draff_N_2_Biochar	700				VFAs +63%			
	Draff_CO_2_Biochar	700				VFAs +28%			
	Wood_Biochar	700				VFAs +29%	Peak rate +70%		
Food waste	Pine sawdust biochar	650	10	35	Sludge heated at 95 °C	H_2 +41%	Peak rate +26%	Buffering pH; facilitating biofilm development	[75]
Food waste	Pine sawdust biochar	650	8.3	35	Heated sludge	H_2 +31%	Peak rate +32% Lag phase −6%	Supporting microbial metabolism and growth; buffering pH	[76]
Cornstalk hydrolysate	Cornstalk residue biochar	300	15	37	*Clostridium* sp. T2	H_2 +170%	Lag phase −40%		[69]
Algae	Algae biochar	600	1.0	37		VFAs +210%		Enhancing electron transport and ATP synthesis	[70]
Organic fraction of municipal solid waste	Wood biochar	500	12.5	37	*Enterobacter aerogenes* and *E. coli*	H_2 +328%	Lag phase −35%	Facilitating biofilm formation and efficient colonization of microbes; ammonia mitigation	[68]
L. digitata	Graphene		1.0	55	Sludge heated at 100 °C	VFAs +53%	Lag phase −47%	Supporting biofilm development; enhancing bacterial electron transfer	This study
	Draff_N_2_Biochar	700				VFAs −17%	Lag phase −36%		
	Draff_CO_2_Biochar	700				VFAs −9%	Lag phase −37%		
	Wood_Biochar	700				VFAs +6%	Lag phase −49%		

functional groups of the carbon materials. These properties of carbon materials were also intrinsically related to each other. A carbonaceous material with a high carbon content, high abundance of sp^2 carbon, and low abundance of oxygen-containing functional groups typically indicated a high graphitic degree, which normally leads to a high EC. It could be inferred that the graphitic carbon core and electrical conductivity of the carbon materials might be crucial parameters in facilitating the fermentation of *L. digitata* by enhancing the bacterial electron transfer. Conductive carbon materials can enhance bacterial metabolism through the stimulation of transmembrane and extracellular electron transfer, which has been demonstrated by the augmentation of representative bacteria *S. oneidensis* with carbon dots [71]. However, further investigation is necessary to reveal the direct fundamental drivers that contribute to the enhanced fermentation and the mechanisms of the carbon-microbes interaction.

Specific surface areas showed no apparent correlations with all fermentation indicators, suggesting that the specific surface area might not be a crucial parameter affecting the fermentation performance. The two draff-derived biochars presented similar elemental compositions. Draff_CO_2_Biochar presented a lower specific surface area and porosity but led to a better fermentation performance such as a shorter lag-phase time and peak fermentation time compared to Draff_N_2_Biochar. This observation was in agreement with Wang et al. [72]. However, this observation did not deny the potential significance of supporting biofilm on the surface of carbon materials. The cell attachment and biofilm development might be a prerequisite to realise the enhancement of bacterial electron transfer as the direct bacterial electron transfer happens on the interface between the bacteria and carbon materials. Cheng et al. demonstrated that bacteria were immobilized on the carbon cloth by comparing the protein attached to the carbon cloth and the protein content in the supernatant [28]. The weak relationship between the specific surface area and the fermentation performance might arise from the fact that the cell attachment occurred principally on the external surface of the additives instead of their

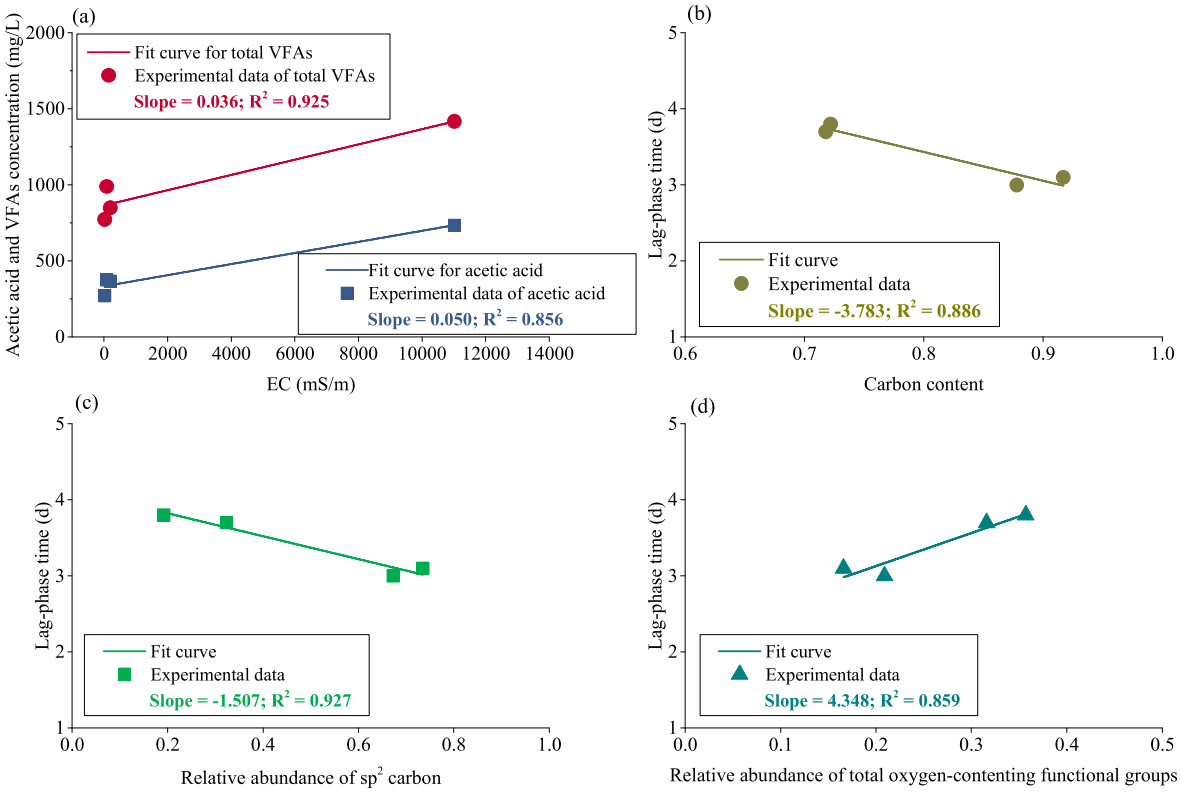


Fig. 9. Correlations between the fermentation performance of *L. digitata* and the biochar properties: (a) Acetic acid and total VFAs production versus the electrical conductivity (EC), (b) Lag-phase time versus the carbon content, (c) Lag-phase time versus the relative abundance of sp^2 carbon, and (d) Lag-phase time versus the relative abundance of total oxygen-containing functional groups.

internal micropores [31].

Based on the discussion, the possible mechanisms for enhancing biohydrogen fermentation with conductive carbon materials were proposed as illustrated in Fig. 10. The conductive carbon materials, particularly graphene and Wood_Biochar, promoted metabolic activities possibly by supporting the development of biofilms and facilitating the transmembrane and extracellular electron transfer. In the absence of conductive materials, the c-type cytochromes are involved in the transmembrane electron transfer and the flavins are involved as a free mediator in the extracellular electron transfer. Their co-existence could indicate the formation of an electron transfer pathway between electroactive bacteria in fermentation systems. It has been proven that extracellular electron transfer could be conducted directly by conductive carbon materials between electroactive microorganisms [73]. The replacement of conductive secreta by conductive carbon materials could possibly reduce the consumption of energy/matter for electron transfer, which may be an important reason for improving the hydrogen production efficiency [74].

Further integration of the fermentation with other valorisation processes will enhance both economic and environmental benefits of the addition of carbon materials. As outlined in a previous study, the enhanced production of carboxylic acids (such as acetic acid and butyric acid) can not only lead to a higher economic return compared with biomethane, but also can serve as versatile precursors for even higher-valued chemical synthesis, such as medium-chain carboxylic acids, polyhydroxyalkanoates, single-cell proteins, and multi-carbon alkanes [4]. In addition to the acceleration of biohydrogen and VFA production, the addition of carbon materials in fermentation may also lead to a range of co-benefits, such as enhancing the process stability, improving the feedstock biodegradability, and offering biofertilizer production (the presence of biochar in digestate can increase soil organic carbon when applied to land at the end of the supply chain [77]). However, the following challenges need to be addressed before the implementation of large-scale application: (1) the understanding of the mechanisms of the carbon-microbes interaction needs to be improved to optimise the yield, production selectivity, and fermentation performance; (2) the net gains from hydrogen and other desirable products have to offset the energy cost for the production and application of carbon materials to achieve economical sustainability; (3) when the enhanced fermentation process is further integrated with other bio/thermo/electrochemical processes, the carbon footprint of the cascading circular bioenergy systems needs to be assessed to verify the environmental sustainability.

4. Conclusion

This study investigated the effects of four carbon materials on facilitating biohydrogen fermentation of glucose, cellulose, and seaweed *L. digitata*. The impacts of the carbon materials varied among different carbon materials and different feedstocks. In the fermentation of glucose, graphene and Wood_Biochar improved the VFAs production by 75% and 29%, respectively. Polysaccharide cellulose proved a difficult substrate for hydrogen fermentative bacteria; thus, the fermentation of cellulose was not enhanced by the carbon additives. All the carbon materials significantly reduced the lag-phase time for fermentation of *L. digitata*. Graphene and Wood_Biochar reduced the lag-phase time by 47% and 49%, respectively. Correlations between the fermentation parameters of *L. digitata* and the properties of the carbon materials (such as the

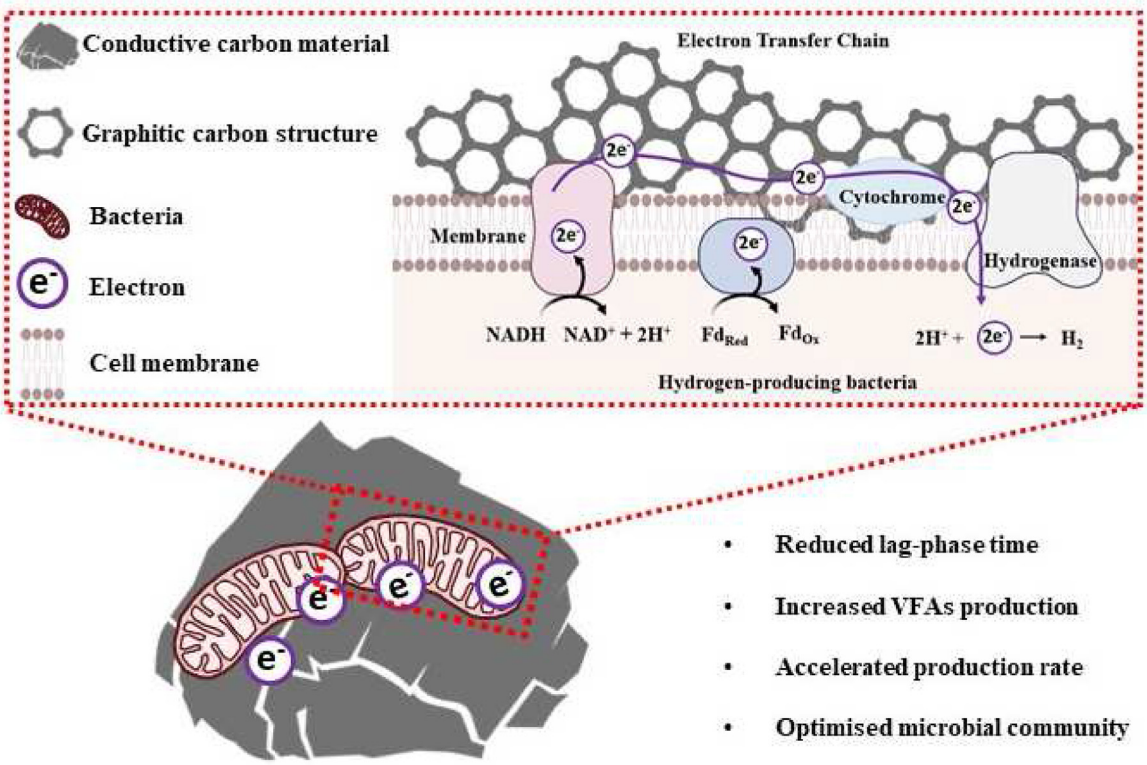


Fig. 10. Proposed role of conductive carbon materials in the hydrogen fermentation.

carbon content, relative abundance of sp^2 carbon and total oxygen-containing functional groups, and electrical conductivity) suggested that the graphitic carbon core and electrical conductivity might play an important role in facilitating the fermentation. The possible mechanisms were postulated as the support for biofilms and the enhancement of the transmembrane and extracellular electron transfer induced by carbonaceous additives.

Declaration of competing interest

The authors declare that they have no known competing financial interests or personal relationships that could have appeared to influence the work reported in this paper.

Acknowledgement

This study was funded by Science Foundation Ireland (SFI) through the Centre for Energy, Climate, Marine (MaREI) under Grant No. 12/RC/2302_P2 and 16/SP/3829, the European Regional Development Fund under the Interreg NWE Project BioWILL (No. NWE 964), the Environmental Protection Agency – Ireland (2018-RE-MS-13), and Sustainable Energy Authority Ireland (RDD/00454). Industrial co-funding from Gas Networks Ireland through the Gas Innovation Group is also gratefully acknowledged.

Appendix A. Supplementary data

Supplementary data to this article can be found online at https://doi.org/10.1016/j.energy.2021.122188.

Credit author statement

Chen Deng: Conceptualization; Methodology; Investigation; Writing – original draft. Richen Lin: Conceptualization; Methodology; Writing – review & editing; Funding acquisition. Xihui Kang: Investigation; Writing – review & editing. Benteng Wu: Investigation; Writing – review & editing. David M Wall: Validation; Writing – review & editing; Funding acquisition. Jerry D Murphy: Conceptualization; Validation; Supervision; Funding acquisition; Writing – review & editing.

References

[1] European Commission. A hydrogen strategy for a climate-neutral Europe. EU; 2020.
[2] Davis SJ, Lewis NS, Shaner M, Aggarwal S, Arent D, Azevedo IL, et al. Net-zero emissions energy systems. Science 2018;360.
[3] Kakoulaki G, Kougias I, Taylor N, Dolci F, Moya J, Jäger-Waldau A. Green hydrogen in Europe – a regional assessment: substituting existing production with electrolysis powered by renewables. Energy Convers Manag 2021:228.
[4] Lin R, Deng C, Zhang W, Hollmann F, Murphy JD. Production of bio-alkanes from biomass and CO2. Trends Biotechnol 2021;39:370–80.
[5] Deng C, Lin R, Kang X, Wu B, O'Shea R, Murphy JD. Improving gaseous biofuel yield from seaweed through a cascading circular bioenergy system integrating anaerobic digestion and pyrolysis. Renew Sustain Energy Rev 2020;128.
[6] D'Adamo I. Adopting a circular economy: current practices and future perspectives. Soc Sci 2019;8.
[7] Sorgulu F, Dincer I. Development of a hythane based cogeneration system integrated with gasification and landfill subsystems. Energy 2021:215.
[8] Lee J-H, Lee D-G, Park J-I, Kim J-Y. Bio-hydrogen production from a marine brown algae and its bacterial diversity. Kor J Chem Eng 2010;27:187–92.
[9] Guneratnam AJ, Xia A, Murphy JD. Comparative study of single- and two-stage fermentation of the brown seaweed Laminaria digitata. Energy Convers Manag 2017;148:405–12.
[10] Jung KW, Kim DH, Shin HS. Fermentative hydrogen production from Laminaria japonica and optimization of thermal pretreatment conditions. Bioresour Technol 2011;102:2745–50.
[11] Liu H, Wang G. Fermentative hydrogen production from macro-algae Laminaria japonica using anaerobic mixed bacteria. Int J Hydrogen Energy 2014;39:9012–7.
[12] Ding L, Cheng J, Lin R, Deng C, Zhou J, Murphy JD. Improving biohydrogen and biomethane co-production via two-stage dark fermentation and anaerobic digestion of the pretreated seaweed Laminaria digitata. J Clean Prod 2020:251.

[13] Xia A, Jacob A, Herrmann C, Tabassum MR, Murphy JD. Production of hydrogen, ethanol and volatile fatty acids from the seaweed carbohydrate mannitol. Bioresour Technol 2015;193:488–97.
[14] Lui J, Chen W-H, Tsang DCW, You S. A critical review on the principles, applications, and challenges of waste-to-hydrogen technologies. Renew Sustain Energy Rev 2020;134.
[15] Xia A, Murphy JD. Microalgal cultivation in treating liquid digestate from biogas systems. Trends Biotechnol 2016;34:264–75.
[16] Tabassum MR, Xia A, Murphy JD. Potential of seaweed as a feedstock for renewable gaseous fuel production in Ireland. Renew Sustain Energy Rev 2017;68:136–46.
[17] Xia A, Cheng J, Song W, Su H, Ding L, Lin R, et al. Fermentative hydrogen production using algal biomass as feedstock. Renew Sustain Energy Rev 2015;51:209–30.
[18] Dinesh Kumar M, Yukesh Kannah R, Kumar G, Sivashanmugam P, Rajesh Banu J. A novel energetically efficient combinative microwave pretreatment for achieving profitable hydrogen production from marine macro algae (Ulva reticulate). Bioresour Technol 2020;301:122759.
[19] Shao W, Wang Q, Rupani PF, Krishnan S, Ahmad F, Rezania S, et al. Biohydrogen production via thermophilic fermentation: a prospective application of Thermotoga species. Energy 2020:197.
[20] Song B, Lin R, Lam CH, Wu H, Tsui T-H, Yu Y. Recent advances and challenges of inter-disciplinary biomass valorization by integrating hydrothermal and biological techniques. Renew Sustain Energy Rev 2021;135.
[21] Cavalcante WA, Gehring TA, Zaiat M. Stimulation and inhibition of direct interspecies electron transfer mechanisms within methanogenic reactors by adding magnetite and granular actived carbon. Chem Eng J 2021:415.
[22] Guo X, Chen H, Zhu X, Xia A, Liao Q, Huang Y, et al. Revealing the role of conductive materials on facilitating direct interspecies electron transfer in syntrophic methanogenesis: a thermodynamic analysis. Energy 2021:229.
[23] Lin R, Cheng J, Ding L, Song W, Liu M, Zhou J, et al. Enhanced dark hydrogen fermentation by addition of ferric oxide nanoparticles using Enterobacter aerogenes. Bioresour Technol 2016;207:213–9.
[24] Lin R, Cheng J, Ding L, Murphy JD. Improved efficiency of anaerobic digestion through direct interspecies electron transfer at mesophilic and thermophilic temperature ranges. Chem Eng J 2018;350:681–91.
[25] Zhan W, Li L, Tian Y, Lei Y, Zuo W, Zhang J, et al. Insight into the roles of ferric chloride on short-chain fatty acids production in anaerobic fermentation of waste activated sludge: performance and mechanism. Chem Eng J 2021:420.
[26] Yang G, Wang J. Various additives for improving dark fermentative hydrogen production: a review. Renew Sustain Energy Rev 2018;95:130–46.
[27] Cheng J, Li H, Ding L, Zhou J, Song W, Li Y-Y, et al. Improving hydrogen and methane co-generation in cascading dark fermentation and anaerobic digestion: the effect of magnetite nanoparticles on microbial electron transfer and syntrophism. Chem Eng J 2020;397.
[28] Cheng J, Li H, Zhang J, Ding L, Ye Q, Lin R. Enhanced dark hydrogen fermentation of Enterobacter aerogenes/HoxEFUYH with carbon cloth. Int J Hydrogen Energy 2019;44:3560–8.
[29] Zhang J, Fan C, Zang L. Improvement of hydrogen production from glucose by ferrous iron and biochar. Bioresour Technol 2017;245:98–105.
[30] Wu J, Dong L, Zhou C, Liu B, Xing D, Feng L, et al. Enhanced butanol-hydrogen coproduction by Clostridium beijerinckii with biochar as cell's carrier. Bioresour Technol 2019;294:122141.
[31] Lu JH, Chen C, Huang C, Zhuang H, Leu SY, Lee DJ. Dark fermentation production of volatile fatty acids from glucose with biochar amended biological consortium. Bioresour Technol 2020;303:122921.
[32] Deng C, Lin R, Cheng J, Murphy JD. Can acid pre-treatment enhance biohydrogen and biomethane production from grass silage in single-stage and two-stage fermentation processes? Energy Convers Manag 2019;195:738–47.
[33] Deng C, Lin RC, Cheng J, Murphy JD. Can acid pre-treatment enhance biohydrogen and biomethane production from grass silage in single-stage and two-stage fermentation processes? Energy Convers Manag 2019;195:738–47.
[34] Eaton AD, Clesceri LS, Greenberg AE, Franson MAH. Standard methods for the examination of water and wastewater. Am J Public Health Nation's Health 1995;56:387–8.
[35] Zhao Z, Zhang Y, Yu Q, Dang Y, Li Y, Quan X. Communities stimulated with ethanol to perform direct interspecies electron transfer for syntrophic metabolism of propionate and butyrate. Water Res 2016;102:475–84.
[36] Wu B, Lin R, Kang X, Deng C, Xia A, Dobson ADW, et al. Graphene addition to digestion of thin stillage can alleviate acidic shock and improve biomethane production. ACS Sustainable Chem Eng 2020;8:13248–60.
[37] Kang X, Lin R, O'Shea R, Deng C, Li L, Sun Y, et al. A perspective on decarbonizing whiskey using renewable gaseous biofuel in a circular bioeconomy process. J Clean Prod 2020.
[38] Chiappero M, Norouzi O, Hu M, Demichelis F, Berruti F, Maria FD, et al. Review of biochar role as additive in anaerobic digestion processes. Renew Sustain Energy Rev 2020;131:110037.
[39] Deng Z, Xia A, Liao Q, Zhu X, Huang Y, Fu Q. Laccase pretreatment of wheat straw: effects of the physicochemical characteristics and the kinetics of enzymatic hydrolysis. Biotechnol Biofuels 2019;12:159.
[40] Özçimen D, Ersoy-Meriçboyu A. Characterization of biochar and bio-oil samples obtained from carbonization of various biomass materials. Renew Energy 2010;35:1319–24.
[41] Silva CHB, Ferreira DC, Ando RA, Temperini MLA. Aniline-1,4-benzoquinone as a model system for the characterization of products from aniline oligomerization in low acidic media. Chem Phys Lett 2012;551:130–3.
[42] Blyth RIR, Buqa H, Netzer FP, Ramsey MG, Besenhard JO, Golob P, et al. XPS studies of graphite electrode materials forlithium ion batteries. Appl Surf Sci 2000;167:99–106.
[43] Miao Z, Huang Y, Xin J, Su X, Sang Y, Liu H, et al. High-performance symmetric supercapacitor constructed using carbon cloth boosted by engineering oxygen-containing functional groups. ACS Appl Mater Interfaces 2019;11:18044–50.
[44] Qi Y, Ge B, Zhang Y, Jiang B, Wang C, Akram M, et al. Three-dimensional porous graphene-like biochar derived from Enteromorpha as a persulfate activator for sulfamethoxazole degradation: role of graphitic N and radicals transformation. J Hazard Mater 2020;399:123039.
[45] Lian F, Cui G, Liu Z, Duo L, Zhang G, Xing B. One-step synthesis of a novel N-doped microporous biochar derived from crop straws with high dye adsorption capacity. J Environ Manag 2016;176:61–8.
[46] Liu Y, Dai G, Zhu L, Wang S. Green conversion of microalgae into high-performance sponge-like nitrogen-enriched carbon. ChemElectroChem 2019;6.602-602.
[47] Engliman NS, Abdul PM, Wu S-Y, Jahim JM. Influence of iron (II) oxide nanoparticle on biohydrogen production in thermophilic mixed fermentation. Int J Hydrogen Energy 2017;42:27482–93.
[48] Akutsu Y, Lee D-Y, Chi Y-Z, Li Y-Y, Harada H, Yu H-Q. Thermophilic fermentative hydrogen production from starch-wastewater with bio-granules. Int J Hydrogen Energy 2009;34:5061–71.
[49] Ding L, Chan Gutierrez E, Cheng J, Xia A, O'Shea R, Guneratnam AJ, et al. Assessment of continuous fermentative hydrogen and methane co-production using macro- and micro-algae with increasing organic loading rate. Energy 2018;151:760–70.
[50] Arellano-García L, Velázquez-Fernández JB, Macías-Muro M, Marino-Marmolejo EN. Continuous hydrogen production and microbial community profile in the dark fermentation of tequila vinasse: response to increasing loading rates and immobilization of biomass. Biochem Eng J 2021:172.
[51] Zhang J, Zhao W, Yang J, Li Z, Zhang J, Zang L. Comparison of mesophilic and thermophilic dark fermentation with nickel ferrite nanoparticles supplementation for biohydrogen production. Bioresour Technol 2021;329:124853.
[52] Xia Y, Cai L, Zhang T, Fang HHP. Effects of substrate loading and co-substrates on thermophilic anaerobic conversion of microcrystalline cellulose and microbial communities revealed using high-throughput sequencing. Int J Hydrogen Energy 2012;37:13652–9.
[53] Sun C, Xia A, Liao Q, Fu Q, Huang Y, Zhu X, et al. Improving production of volatile fatty acids and hydrogen from microalgae and rice residue: effects of physicochemical characteristics and mix ratios. Appl Energy 2018;230:1082–92.
[54] Zhao L, Wu KK, Chen C, Ren HY, Wang ZH, Nan J, et al. Role of residue cornstalk derived biochar for the enhanced bio-hydrogen production via simultaneous saccharification and fermentation of cornstalk. Bioresour Technol 2021;330:125006.
[55] Xia A, Jacob A, Tabassum MR, Herrmann C, Murphy JD. Production of hydrogen, ethanol and volatile fatty acids through co-fermentation of macro- and micro-algae. Bioresour Technol 2016;205:118–25.
[56] Yang G, Yin Y, Wang J. Microbial community diversity during fermentative hydrogen production inoculating various pretreated cultures. Int J Hydrogen Energy 2019;44:13147–56.
[57] Zhao W, Zhang J, Zhang H, Yang M, Zang L. Comparison of mesophilic and thermophilic biohydrogen production amended by nickel-doped magnetic carbon. J Clean Prod 2020:270.
[58] Lu JH, Chen C, Huang C, Lee DJ. Glucose fermentation with biochar-amended consortium: microbial consortium shift. Bioengineered 2020;11:272–80.
[59] Wang Y, Xi B, Li M, Jia X, Wang X, Xu P, et al. Hydrogen production performance from food waste using piggery anaerobic digested residues inoculum in long-term systems. Int J Hydrogen Energy 2020;45:33208–17.
[60] Akhlaghi M, Boni MR, De Gioannis G, Muntoni A, Polettini A, Pomi R, et al. A parametric response surface study of fermentative hydrogen production from cheese whey. Bioresour Technol 2017;244:473–83.
[61] Yang G, Wang J. Changes in microbial community structure during dark fermentative hydrogen production. Int J Hydrogen Energy 2019;44:25542–50.
[62] Chen J, Liu Y, Liu K, Hu L, Yang J, Wang X, et al. Bacterial community composition of internal circulation reactor at different heights for large-scale brewery wastewater treatment. Bioresour Technol 2021;331:125027.
[63] Zhang K, Cao G-L, Ren N-Q. Bioaugmentation with Thermoanaerobacterium thermosaccharolyticum W16 to enhance thermophilic hydrogen production using corn stover hydrolysate. Int J Hydrogen Energy 2019;44:5821–9.
[64] Jia X, Wang Y, Ren L, Li M, Tang R, Jiang Y, et al. Early warning indicators and microbial community dynamics during unstable stages of continuous hydrogen production from food wastes by thermophilic dark fermentation. Int J Hydrogen Energy 2019;44:30000–13.
[65] Strazzera G, Battista F, Tonanzi B, Rossetti S, Bolzonella D. Optimization of short chain volatile fatty acids production from household food waste for biorefinery applications. Environmental Technology & Innovation 2021:23.
[66] Silva V, Ratti RP, Sakamoto IK, Andrade MVF, Varesche MBA. Biotechnological products in batch reactors obtained from cellulose, glucose and xylose using thermophilic anaerobic consortium. Renew Energy 2018;125:537–45.
[67] Althuri A, Venkata Mohan S. Sequential and consolidated bioprocessing of biogenic municipal solid waste: a strategic pairing of thermophilic anaerobe

and mesophilic microaerobe for ethanol production. Bioresour Technol 2020;308:123260.
[68] Sharma P, Melkania U. Biochar-enhanced hydrogen production from organic fraction of municipal solid waste using co-culture of Enterobacter aerogenes and E. coli. Int J Hydrogen Energy 2017;42:18865–74.
[69] Zhao L, Chen C, Ren HY, Wu JT, Meng J, Nan J, et al. Feasibility of enhancing hydrogen production from cornstalk hydrolysate anaerobic fermentation by RCPH-biochar. Bioresour Technol 2020;297:122505.
[70] Duan X, Chen Y, Yan Y, Feng L, Chen Y, Zhou Q. New method for algae comprehensive utilization: algae-derived biochar enhances algae anaerobic fermentation for short-chain fatty acids production. Bioresour Technol 2019;289:121637.
[71] Yang C, Aslan H, Zhang P, Zhu S, Xiao Y, Chen L, et al. Carbon dots-fed Shewanella oneidensis MR-1 for bioelectricity enhancement. Nat Commun 2020;11:1379.
[72] Wang G, Li Q, Dzakpasu M, Gao X, Yuwen C, Wang XC. Impacts of different biochar types on hydrogen production promotion during fermentative co-digestion of food wastes and dewatered sewage sludge. Waste Manag 2018;80:73–80.
[73] Wu Y, Wang S, Liang D, Li N. Conductive materials in anaerobic digestion: from mechanism to application. Bioresour Technol 2019:122403.
[74] Bu J, Wei HL, Wang YT, Cheng JR, Zhu MJ. Biochar boosts dark fermentative H2 production from sugarcane bagasse by selective enrichment/colonization of functional bacteria and enhancing extracellular electron transfer. Water Res 2021;202:117440.
[75] Sunyoto NMS, Zhu M, Zhang Z, Zhang D. Effect of biochar addition and initial pH on hydrogen production from the first phase of two-phase Anaerobic digestion of carbohydrates food waste. Energy Procedia 2017;105:379–84.
[76] Sunyoto NMS, Zhu M, Zhang Z, Zhang D. Effect of biochar addition on hydrogen and methane production in two-phase anaerobic digestion of aqueous carbohydrates food waste. Bioresour Technol 2016;219:29–36.
[77] Masebinu SO, Akinlabi ET, Muzenda E, Aboyade AO. A review of biochar properties and their roles in mitigating challenges with anaerobic digestion. Renew Sustain Energy Rev 2019;103:291–307.